Editors' Suggestion

Liquid-Solid Slip on Charged Walls: The Dramatic Impact of Charge Distribution

Yanbo Xie,[1,*] Li Fu,[2,*] Thomas Niehaus,[3] and Laurent Joly[3,4,†]

[1]MOE Key Laboratory of Material Physics and Chemistry under Extraordinary Conditions, School of Physical Science and Technology, Northwestern Polytechnical University, Xian, 710072, China

[2]Univ Lyon, Ecole Centrale de Lyon, Laboratoire de Tribologie et Dynamique des Systèmes, UMR 5513, 36 avenue Guy de Collongue, 69134 Ecully Cedex, France

[3]Univ Lyon, Université Claude Bernard Lyon 1, CNRS, Institut Lumière Matière, F-69622, Villeurbanne, France

[4]Institut Universitaire de France (IUF), 1 rue Descartes, 75005 Paris, France

(Received 7 February 2020; revised 24 April 2020; accepted 12 June 2020; published 29 June 2020)

Nanofluidic systems show great promise for applications in energy conversion, where their performance can be enhanced by nanoscale liquid-solid slip. However, efficiency is also controlled by surface charge, which is known to reduce slip. Combining molecular dynamics simulations and analytical developments, we show the dramatic impact of surface charge distribution on the slip-charge coupling. Homogeneously charged graphene exhibits a very favorable slip-charge relation (rationalized with a new theoretical model correcting some weaknesses of the existing ones), leading to giant electrokinetic energy conversion. In contrast, slip is strongly affected on heterogeneously charged surfaces, due to the viscous drag induced by counterions trapped on the surface. In that case slip should depend on the detailed physical chemistry of the interface controlling the fraction of bound ions. Our numerical results and theoretical models provide new fundamental insight into the molecular mechanisms of liquid-solid slip, and practical guidelines for searching new functional interfaces with optimal energy conversion properties, e.g., for blue energy or waste heat harvesting.

DOI: 10.1103/PhysRevLett.125.014501

Introduction.—The development of sustainable alternative energies is one of the greatest challenges faced by our society, and nanofluidic systems could contribute significantly in that field [1–5]. For instance, membranes with nanoscale porosity could be used to harvest energy from the salinity difference between sea and river water [6–8] or from waste heat [9,10]. Energy conversion in nanofluidic systems originates at liquid-solid interfaces, where the properties of the liquid differ from their bulk value [11,12]. In particular, in aqueous electrolytes, the so-called electrokinetic (EK) effects—coupling different types of applied forcing and induced flux—are controlled by hydrodynamics and electrostatics in the electrical double layer (EDL), a nanometric charged layer of liquid in contact with charged walls [13–15]. Consequently, the EK response of an interface is largely controlled by the wall surface charge [16]. Yet, nanoscale liquid-solid slip [17,18] can amplify EK effects [19–27]. Slip is quantified through the Navier boundary condition, balancing the viscous shear stress at the wall, $\eta\partial_z v|_{z=z_w}$ (with η the viscosity and $\partial_z v|_{z=z_w}$ the shear rate at the wall), and a liquid-solid friction stress λv_s (with v_s the slip velocity and λ the fluid friction coefficient) [28,29]. The Navier boundary condition is usually rewritten as $v_s = b\partial_z v|_{z=z_w}$, defining the so-called slip length $b = \eta/\lambda$ [17].

In the presence of slip, the EK response is amplified by a factor $1 + b/L$, where L is the thickness of the interfacial layer (e.g., the Debye length λ_D for the EDL) [12,22,30,31]. For optimal performance, it is therefore critical to use surfaces with both a large surface charge and a large slip length. With that regard, it has been shown that the slip length decreases when surface charge increases [32–35], which impacts the EK energy conversion efficiency [36]. The slip-charge coupling has been investigated both theoretically and experimentally over the recent years [37–43]; in particular, a theoretical description has been proposed [32] for model surfaces with a homogeneous charge, which can arise from the polarization of a conductive surface, analogous to, e.g., the charging of amorphous carbon electrodes in supercapacitors [44–47]. However, for most surfaces, charge arises from the dissociation of surface groups or specific adsorption of charged species, resulting in a spatially heterogeneous charge. Both experiments and simulations have shown that lateral heterogeneity of surface charge can have a strong impact on the interfacial water structure [48,49], and in general, it is not clear that the existing theoretical description of slip-charge coupling [32] is suitable to describe heterogeneous surfaces.

In that context, we used molecular dynamics (MD) simulations to investigate the impact of surface charge distribution on liquid-solid slip, with the goal to understand and optimize the slip-charge dependency. To that aim we considered a model interface between aqueous sodium chloride and charged graphene. We observed a dramatic

impact of the surface charge distribution, which we rationalized through analytical modeling. We then explored the consequences of charge distribution on slip-enhanced EK energy conversion, and predicted a giant performance of polarized graphene.

Systems and methods.—We conducted MD simulations with the LAMMPS package [50] to investigate the change of slip length as a function of both the surface charge density and its distribution. Here, we present the main features of the simulation setup; technical details can be found in the Supplemental Material (SM) [51]. We considered an aqueous NaCl solution confined between two parallel graphene sheets. Previous MD work [32,33,59] has shown that the slip-charge coupling was not significantly affected by the salt concentration, and here we used a constant concentration $\rho_s \sim 1.3M$ in all configurations, unless specified. The corresponding Debye length λ_D was ca. 0.26 nm. The distance between the graphene sheets was ~10 times larger than λ_D, so that the EDLs of both walls were well separated. We used periodic boundary conditions in the x and y directions parallel to the sheets, with a lateral box size of ca. 3.5 nm. We simulated both homogeneously and heterogeneously charged graphene walls, with surface charge density Σ from -0.06 to 0 C/m^2 (see Fig. 1). We also considered surfaces with a positive charge, and obtained identical results for homogeneous charge, but different results for heterogeneous charge, as discussed later. On homogeneously charged ("polarized") walls with a surface area of A, each atom on a wall was charged by q/N, where $q = \Sigma \times A$ is the total charge and N is the total number of carbon atoms on the wall. The maximum charge per atom, obtained for $|\Sigma| = 0.06$ mC/m^2, was $\sim 0.01e$. We checked using density functional based tight binding [60] simulations that the graphene structure was barely modified by such a charge [51]. On heterogeneously charged walls with the same area and charge density, $n = q/e$ random selected carbon atoms were charged by an elementary charge e.

We used the TIP4P/2005 force field [61] for water. Ions were simulated with the scaled-ionic-charge model by Kann and Skinner [62], using a scaling factor of 0.85. For consistency, the charge of wall atoms was rescaled with the same factor as for the ions [63] in the simulation. Nevertheless, we used the unscaled charge for the later calculation of surface charge density. Water and carbon interacted through a recently proposed force field calibrated from high-level quantum calculations of water adsorption on graphene [64]. The systems were maintained at $T = 298$ K and $p = 1$ atm. A Couette flow was generated in the liquid by moving the walls with a constant speed of $|V_x|$ in opposite directions along the x axis ($|V_x| = 10$–50 m/s). We employed the same method discussed in Ref. [65] to compute the slip length [51].

Results and discussion.—Figure 2(a) shows the evolution of b as a function of the surface charge density $|\Sigma|$, for homogeneously and heterogeneously charged graphene walls. For comparison, results from Ref. [33] obtained with a generic hydrophobic surface are also shown. Consistently with previous MD results on graphitic

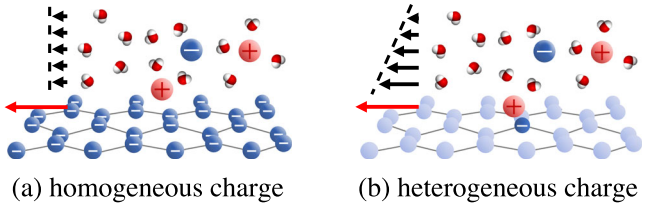

FIG. 1. Two surface charge distributions were considered in this work: (a) homogeneous charge, with all surface atoms baring the same partial charge ("polarized wall"); (b) heterogeneous charge, with a fraction of surface atoms baring an elementary charge.

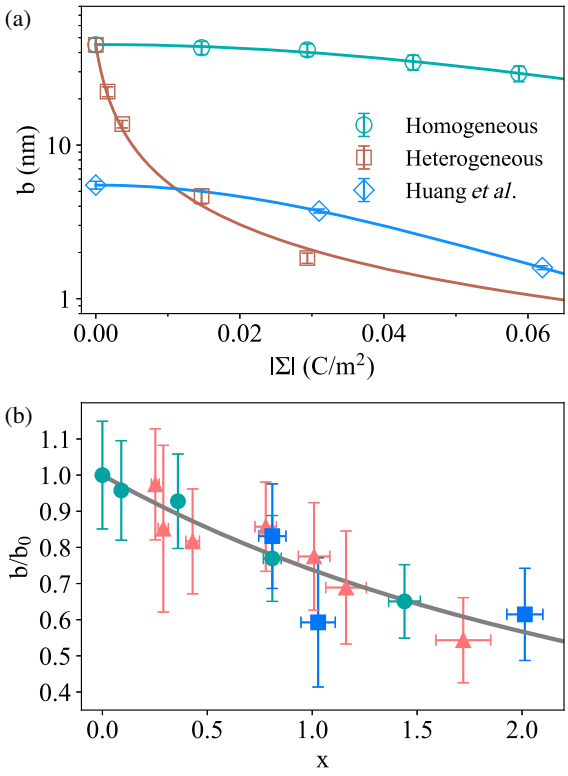

FIG. 2. (a) Slip length b versus surface charge density $|\Sigma|$: simulation results for homogeneously (green circles) and heterogeneously (brown squares) charged graphene, and for a generic hydrophobic wall with homogeneous charge (blue diamonds, taken from Ref. [33]); Green and blue lines are fits with Eq. (1), and the brown line is a fit with Eq. (2). (b) Slip length on homogeneously charged surfaces normalized by the uncharged value b/b_0 as a function of the dimensionless parameter x in Eq. (1); simulation results for graphene (green circles) and graphenelike surfaces, either with different wettability (pink triangles) or strained graphene (blue squares); all results are fitted with Eq. (1), using a single value of $\alpha = 0.165$.

surfaces [66,67], the slip length on uncharged graphene is very large, ca. 45 nm. Upon charging the surface, the slip length decreases, but the effect of surface charge density on slip is dramatically different between the homogeneous and the heterogeneous walls. On polarized graphene, as $|\Sigma|$ increases from 0 to 0.06 C/m^2, b gradually decreases from 45 to 30 nm. On heterogeneously charged graphene, b decays much faster, down by more than a factor of 2 for only 0.015 C/m^2. Finally, comparing the two homogeneous walls, graphene comes out as a more interesting surface than the hydrophobic surface considered in Ref. [33], combining both a larger slip length on the uncharged wall, and a weaker charge dependency.

In order to rationalize the MD results, and identify criteria for optimal slip-charge dependency, we developed two models to describe the homogeneous and heterogeneous cases. For a homogeneous surface charge, we reconsidered a calculation presented in Ref. [32], as detailed in the SM [51]. This calculation is based on a Green-Kubo expression for the liquid-solid friction coefficient λ (related to the slip length through the viscosity: $b = \eta/\lambda$). The Green-Kubo formula relates λ to the fluctuations of the friction force at equilibrium. By separating the electrostatic and the nonelectrostatic contributions to the friction force, one can show that

$$b = \frac{b_0}{(1+\alpha x)^2}, \quad \text{with}$$
$$x = \left(\frac{3\pi\sigma_\ell b_0}{\sigma_s^2}\right)^{1/2}\left(\frac{\ell_B^i}{\sigma_s}\right)\left(\frac{\Sigma\sigma_s^2}{e}\right)^2, \tag{1}$$

where b_0 is the slip length on the neutral surface, α a numerical prefactor, σ_ℓ the effective hydrodynamic diameter of liquid particles, σ_s the wall interatomic distance, and $\ell_B^i = e^2/(4\pi\varepsilon_d^i k_B T)$ the Bjerrum length of the interface (with ε_d^i the dielectric permittivity of the interface). Note that α encompasses the unknown ratio between the corrugation of the tangential electric force and the characteristic normal electric field, which should, in particular, depend on the crystallographic structure of the wall. As discussed in Ref. [33], because friction arises mainly from interactions between the first liquid adsorption layer and the solid surface, the dielectric permittivity and corresponding Bjerrum length ℓ_B^i in Eq. (1) should be those of the vacuum gap separating these two layers: $\ell_B^i = \ell_B^0 \approx 55.8$ nm at room temperature.

To fit the MD results for homogeneous charge with Eq. (1), σ_ℓ was obtained from the Stokes-Einstein relation between TIP4P/2005 water self-diffusion and viscosity, characterized in Ref. [68]: $\sigma_\ell = k_B T/(3\pi\eta D) = 0.214$ nm; σ_s was set to 0.142 nm for graphene, and 0.337 nm for the generic surface. The only free parameters were therefore b_0 and α. Equation (1) fits the MD results very well, using $b_0 = 45.1$ nm and $\alpha = 0.165$ for graphene, and $b_0 = 5.48$ nm and $\alpha = 0.270$ for the generic surface.

In particular, the model shows that the relevant characteristics of the wall controlling the slip-charge dependency are the uncharged slip length (the higher b_0 is, the faster b decreases with Σ) and the wall interatomic distance (the larger σ_s is, the faster b decreases with Σ). For instance, graphene, having a larger uncharged slip length, should display a stronger slip-charge dependency than the LJ wall, but it benefits from a smaller interatomic distance that overcompensates the effect of the uncharged slip length. Therefore, the behavior of graphene, which combines a large uncharged slip length and a weak slip-charge dependency, can be traced back to the unusually small interatomic distance, and should for that reason be quite unique. Nevertheless, Eq. (1) can still be used as a guideline to search for other surfaces with potentially favorable properties.

With that in mind, note that Eq. (1) differs in several aspects from a similar equation introduced previously, Eq. (12) in Ref. [32]. First, this new expression does not rely on the assumption that the electric friction is small as compared to the nonelectric friction. Even in the low surface charge limit, the prefactor in front of Σ^2 scales differently with the uncharged slip length b_0: $b_0^{1/2}$ here versus b_0^1 in the previous formula. Additionally, the present formula now clarifies how the slip length depends on the liquid and solid atomic sizes. To test Eq. (1) further and in particular the predicted impact of b_0 and σ_s, we considered graphenelike surfaces where we varied independently these two parameters. First, we varied the LJ interaction energy between carbon and water atoms without changing the wall structure, in order to change b_0 for a constant σ_s. Second, we considered artificially strained graphene walls, i.e., we changed the interatomic distance σ_s while keeping the same water-carbon interaction energy as for graphene (here b_0 was also affected by the strain). When doing so we also changed the number of wall unit cells in order to keep the surface (and surface charge density Σ) approximately constant, and always recomputed the exact value of Σ [51]. Figure 2(b) compares the predictions of the model and the simulation results, which match quite well and validate the new model (details and a comparison with the previous formula are given in the SM).

We now turn to the heterogeneously charged surfaces. In that case, counterions can strongly bind to the charged sites. In general, the fraction of bound counterions should depend on the details of the surface physical chemistry and ion distribution in the EDL. However, in the specific case of the negatively charged graphene surfaces considered in this work, all counterions were bound to a charged site, and remained trapped during the whole simulation (we checked that this remained true for a lower salt concentration of $\sim 0.13M$). In that case one can consider that the bound counterions belong to the solid surface and effectively cancel the surface charge. Consequently, we can estimate

the slip length as that of a neutral liquid in contact with a neutral wall, build from the charged wall and the bound counterions. The latter protrude over the otherwise smooth surface and generate a Stokes drag, which can be described following a similar derivation used to predict the slip of a liquid over a surfactant layer [59]. As detailed in the SM [51], for monovalent ions one can show that

$$b = \frac{b_0}{1 + 3\pi\sigma_h b_0(|\Sigma|/e)}, \tag{2}$$

where b_0 is the slip length on the uncharged surface, and σ_h the effective hydrodynamic diameter of the counterions, controlling their individual viscous drag.

Equation (2) fits the numerical results very well, using $b_0 = 45.1$ nm as for the homogeneously charged graphene, and $\sigma_h = 0.261$ nm. The fitted effective hydrodynamic diameter σ_h of the counterions is quite reasonable, with a value close to the van der Waals diameter of the ions. Furthermore, we show in the SM [51] that Eq. (2) also describes consistently modified graphene with different wettability or interatomic distance.

However, in general, not all counterions will bind to the wall. In that case, the slip length will not be directly connected to the surface charge, and will be controlled the fraction of bound ions. Through this fraction, the slip length should therefore depend on the specific physical and chemical features of the interface, in contrast with the homogeneous charge case, where only a few well controlled parameters influence slip. As a striking illustration, we simulated heterogeneously charged graphene with a positive charge, see the SM [51]; in that case, Cl^- counterions did not bind to the charged sites, consistently with a previous observation on a similar system by Qiao and Aluru [69], and resulting in a different slip-charge relation.

We now would like to explore the impact of the slip-charge relation on the energy conversion performance of nanofluidic systems. To that aim, we will focus on electromechanical energy conversion at charged surfaces, considering the two reciprocal EK effects of electro-osmotic flows and streaming current [13,14]. Experimentally, the amplitude of EK effects is quantified by the so-called zeta potential—denoted ζ, extracted from macroscopic measurements of the EK response using the Helmholtz-Smoluchowski equation [15,16], which relates the applied forcing and the resulting flux: for electro-osmosis, $v_{eo} = -(\varepsilon_d\zeta/\eta)E_x$ (with E_x the applied electric field, v_{eo} the resulting electro-osmotic velocity, ε_d the dielectric permittivity of the liquid), and for streaming current, $j_e = -(\varepsilon_d\zeta/\eta)(-\nabla p)$ (with $-\nabla p$ the applied pressure gradient, and j_e the resulting electrical current). According to this experimental definition, ζ is a macroscopic response coefficient, arising from the coupling of electrostatics and hydrodynamics in the EDL. As such, it has been shown theoretically and experimentally that the zeta potential can be amplified by liquid-solid slip [19,20,30,31,70,71], and writes [32]

$$\zeta = V_0\left(1 + \frac{b}{\lambda_D^{\text{eff}}}\right) = V_0 + \frac{\Sigma b}{\varepsilon_d}, \tag{3}$$

with V_0 the surface potential, and where $\lambda_D^{\text{eff}} = -V_0/\partial_z V|_{z=z_{\text{wall}}}$ characterizes the thickness of the EDL. The second expression for ζ shows that liquid-solid slip simply adds a contribution $\zeta_{\text{slip}} = \Sigma b/\varepsilon_d$ to the surface potential, which only depends on Σ, b, and ε_d.

For polarized graphene, using Eq. (1) to express b, $|\zeta_{\text{slip}}|$ is predicted to go through a maximum of ~2000 mV, for $|\Sigma| \sim 0.06$ C/m^2 (corresponding to a charge per atom of $\sim 0.01e$, comparable with charges in the amorphous carbon electrodes of supercapacitors [44–47]), see Fig. 3 and the SM [51]. This value exceeds by far usual zeta potentials, which typically saturate around $4k_BT/e \sim 100$ mV. To confirm the prediction of the model, we performed explicit streaming current simulations [51]: we applied a pressure gradient to the liquid, measured the resulting electrical current, and computed the zeta potential using the Helmholtz-Smoluchowski equation. The computed zeta potential indeed matches the theoretical prediction, see Fig. 3. Consequently, polarized graphene appears as an ideal system to evidence experimentally the zeta potential amplification by liquid-solid slip.

For heterogeneously charged graphene with $\Sigma < 0$, all counterions being trapped at the wall, there is no net charge in the liquid, so that the zeta potential must vanish. We performed direct streaming current simulations for $\Sigma = -0.03$ C/m^2 to confirm that prediction and indeed measured a vanishing value within error bars, $\zeta = -3.9 \pm 6.8$ mV.

Of course this result is specific to the systems simulated here. For instance, as shown previously [69], simply reversing the surface charge changes the counterion adsorption behavior, and consequently the zeta potential. In

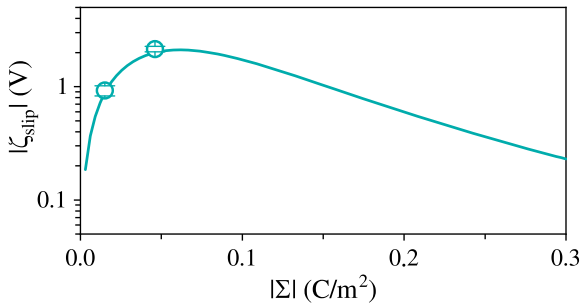

FIG. 3. Zeta potential, quantifying the electrokinetic response of the interface, versus surface charge density for homogeneously charged graphene. The line represents the theoretical prediction for the slip contribution $|\zeta_{\text{slip}}|$; symbols represent measurements through streaming current simulations.

general, when only a fraction of the counterions are trapped [59,72], the zeta potential does not vanish, and it depends on the fraction of bound ions, both directly through the resulting effective surface charge and indirectly through the impact of ion binding on slip.

Conclusion.—Using molecular dynamics simulations and analytical developments, we investigated the impact of surface charge distribution on liquid-solid slip. We focused on model interfaces between aqueous NaCl and graphene. We found a large contrast between surfaces with a homogeneous charge, representative of polarized conductive surfaces, and surfaces with a heterogeneous charge, typically arising from the dissociation of surface groups. On polarized graphene, the slip length is very large and weakly affected by surface charge. Our model rationalizes this exceptional performance and traces it back to the unusually small interatomic distance of graphene. Note that homogeneously charged graphene was modeled with localized charges, while real polarized graphene features delocalized and mobile charges [73,74]. In future work, *ab initio* molecular dynamics [75–78] could help to explore the role of electronic screening effects and image charges on liquid-solid friction, for graphene and more generally for metallic walls [79–81]. On heterogeneously charged graphene with a negative surface charge, Na^+ counterions bind to the charged sites and induce a viscous drag, which strongly decreases the slip length. In contrast, for a positive charge, Cl^- counterions do not bind and the slip length decreases less with surface charge. Overall, for a heterogeneous surface charge, slip should be affected by the specific details of the ion binding equilibrium, and not be directly controlled by the surface charge, making the development of a generic model for slip-charge coupling particularly challenging.

We also predict a giant EK energy conversion on polarized graphene, due to favorable slip-charge dependency. On heterogeneous surfaces, we predict that the EK response should be specific to the physical chemistry of the interface, both directly through the effective surface charge resulting from counterion binding, and indirectly through the impact of bound ions on slip. We hope the simulation results and the models developed to rationalize them will help in the search for functional interfaces with optimal EK response. In particular, our results provide a fundamental framework for a future extensive investigation of the complex coupling between ion binding, slip, and EK response on a variety of realistic surfaces.

The authors thank Cecilia Herrero, Céline Merlet, Mathieu Salanne, and Benjamin Rotenberg for fruitful discussions. This work is supported by the ANR, Project No. ANR-16-CE06-0004-01 NECtAR. Y. X. is supported by NSFC No. U1732143 and Fundamental Research Funds for the Central Universities (Grants No. 3102017jc01001, No. 3102019ghxm020). L. J. is supported by the Institut Universitaire de France.

*These authors contributed equally to this work.
†laurent.joly@univ-lyon1.fr

[1] F. H. J. van der Heyden, D. J. Bonthuis, D. Stein, C. Meyer, and C. Dekker, Electrokinetic energy conversion efficiency in nanofluidic channels, Nano Lett. **6**, 2232 (2006).
[2] S. Pennathur, J. C. T. Eijkel, and A. van den Berg, Energy conversion in microsystems: Is there a role for micro/nanofluidics?, Lab Chip **7**, 1234 (2007).
[3] F. H. Van Der Heyden, D. J. Bonthuis, D. Stein, C. Meyer, and C. Dekker, Power generation by pressure-driven transport of ions in nanofluidic channels, Nano Lett. **7**, 1022 (2007).
[4] W. Sparreboom, A. van den Berg, and J. C. T. Eijkel, Principles and applications of nanofluidic transport, Nat. Nanotechnol. **4**, 713 (2009).
[5] L. Bocquet and P. Tabeling, Physics and technological aspects of nanofluidics, Lab Chip **14**, 3143 (2014).
[6] A. Siria, P. Poncharal, A.-L. Biance, R. Fulcrand, X. Blase, S. T. Purcell, and L. Bocquet, Giant osmotic energy conversion measured in a single transmembrane boron nitride nanotube, Nature (London) **494**, 455 (2013).
[7] J. Feng, M. Graf, K. Liu, D. Ovchinnikov, D. Dumcenco, M. Heiranian, V. Nandigana, N. R. Aluru, A. Kis, and A. Radenovic, Single-layer MoS_2 nanopores as nanopower generators, Nature (London) **536**, 197 (2016).
[8] A. Siria, M.-L. Bocquet, and L. Bocquet, New avenues for the large-scale harvesting of blue energy, Nat. Rev. Chem. **1**, 0091 (2017).
[9] L. Fu, S. Merabia, and L. Joly, Understanding fast and robust thermo-osmotic flows through carbon nanotube membranes: Thermodynamics meets hydrodynamics, J. Phys. Chem. Lett. **9**, 2086 (2018).
[10] L. Fu, L. Joly, and S. Merabia, Giant Thermoelectric Response of Nanofluidic Systems Driven by Water Excess Enthalpy, Phys. Rev. Lett. **123**, 138001 (2019).
[11] J. Anderson, Colloid transport by interfacial forces, Annu. Rev. Fluid Mech. **21**, 61 (1989).
[12] L. Bocquet and E. Charlaix, Nanofluidics, from bulk to interfaces, Chem. Soc. Rev. **39**, 1073 (2010).
[13] D. Andelman, Electrostatic Properties of Membranes: The Poisson-Boltzmann Theory, in *Handbook of Biological Physics* Vol. 1B (Elsevier, 1995), pp. 603–642.
[14] R. J. Hunter, *Foundations of Colloid Science* (Oxford University Press, 2001).
[15] R. Hartkamp, A.-L. Biance, L. Fu, J.-F. Dufrêche, O. Bonhomme, and L. Joly, Measuring surface charge: Why experimental characterization and molecular modeling should be coupled, Curr. Opin. Colloid Interface Sci. **37**, 101 (2018).
[16] A. Delgado, F. Gonzâlez-Caballero, R. Hunter, L. Koopal, and J. Lyklema, Measurement and interpretation of electrokinetic phenomena, J. Colloid Interface Sci. **309**, 194 (2007).
[17] L. Bocquet and J.-L. Barrat, Flow boundary conditions from nano- to micro-scales, Soft Matter **3**, 685 (2007).
[18] P. J. Daivis and B. D. Todd, Challenges in nanofluidics-beyond Navier-Stokes at the molecular scale, Processes **6**, 1 (2018).
[19] V. Marry, J.-F. Dufrêche, M. Jardat, and P. Turq, Equilibrium and electrokinetic phenomena in charged porous media

from microscopic and mesoscopic models: Electro-osmosis in montmorillonite, Mol. Phys. **101**, 3111 (2003).
[20] L. Joly, C. Ybert, E. Trizac, and L. Bocquet, Hydrodynamics Within the Electric Double Layer on Slipping Surfaces, Phys. Rev. Lett. **93**, 257805 (2004).
[21] J.-F. Dufrêche, V. Marry, N. Malikova, and P. Turq, Molecular hydrodynamics for electro-osmosis in clays: From Kubo to Smoluchowski, J. Mol. Liq. **118**, 145 (2005).
[22] A. Ajdari and L. Bocquet, Giant Amplification of Interfacially Driven Transport by Hydrodynamic Slip: Diffusio-Osmosis and Beyond, Phys. Rev. Lett. **96**, 186102 (2006).
[23] Y. Ren and D. Stein, Slip-enhanced electrokinetic energy conversion in nanofluidic channels, Nanotechnology **19**, 195707 (2008).
[24] S. R. Maduar, A. V. Belyaev, V. Lobaskin, and O. I. Vinogradova, Electrohydrodynamics Near Hydrophobic Surfaces, Phys. Rev. Lett. **114**, 118301 (2015).
[25] L. Fu, S. Merabia, and L. Joly, What Controls Thermo-osmosis? Molecular Simulations Show the Critical Role of Interfacial Hydrodynamics, Phys. Rev. Lett. **119**, 214501 (2017).
[26] E. F. Silkina, E. S. Asmolov, and O. I. Vinogradova, Electro-osmotic flow in hydrophobic nanochannels, Phys. Chem. Chem. Phys. **21**, 23036 (2019).
[27] B. L. Werkhoven and R. van Roij, Coupled water, charge and salt transport in heterogeneous nano-fluidic systems, Soft Matter **16**, 1527 (2020).
[28] C. Navier, Mémoire sur les lois du mouvement des fluides, Mem. Acad. Sci. Inst. Fr. **6**, 389 (1823).
[29] B. Cross, C. Barraud, C. Picard, L. Léger, F. Restagno, and E. Charlaix, Wall slip of complex fluids: Interfacial friction versus slip length, Phys. Rev. Fluids **3**, 062001 (2018).
[30] V. M. Muller, I. P. Sergeeva, V. D. Sobolev, and N. V. Churaev, Boundary effects in the theory of electrokinetic phenomena, Colloid J. USSR **48**, 606 (1986).
[31] H. A. Stone, A. D. Stroock, and A. Ajdari, Engineering flows in small devices: Microfluidics toward a lab-on-a-chip, Annu. Rev. Fluid Mech. **36**, 381 (2004).
[32] L. Joly, C. Ybert, E. Trizac, and L. Bocquet, Liquid friction on charged surfaces: From hydrodynamic slippage to electrokinetics, J. Chem. Phys. **125**, 204716 (2006).
[33] D. M. Huang, C. Cottin-Bizonne, C. Ybert, and L. Bocquet, Aqueous electrolytes near hydrophobic surfaces: Dynamic effects of ion specificity and hydrodynamic slip, Langmuir **24**, 1442 (2008).
[34] A. Boţan, V. Marry, B. Rotenberg, P. Turq, and B. Noetinger, How electrostatics influences hydrodynamic boundary conditions: Poiseuille and electro-osmostic flows in clay nanopores, J. Phys. Chem. C **117**, 978 (2013).
[35] D. Jing and B. Bhushan, The coupling of surface charge and boundary slip at the solid-liquid interface and their combined effect on fluid drag: A review, J. Colloid Interface Sci. **454**, 152 (2015).
[36] C. Bakli and S. Chakraborty, Electrokinetic energy conversion in nanofluidic channels: Addressing the loose ends in nanodevice efficiency, Electrophoresis **36**, 675 (2015).
[37] D. Jing and B. Bhushan, Quantification of surface charge density and its effect on boundary slip, Langmuir **29**, 6953 (2013).
[38] Y. Pan and B. Bhushan, Role of surface charge on boundary slip in fluid flow, J. Colloid Interface Sci. **392**, 117 (2013).
[39] Y. Li and B. Bhushan, The effect of surface charge on the boundary slip of various oleophilic/phobic surfaces immersed in liquids, Soft Matter **11**, 7680 (2015).
[40] J. Catalano, R. G. H. Lammertink, and P. M. Biesheuvel, Theory of fluid slip in charged capillary nanopores, arXiv:1603.09293.
[41] P. Simonnin, V. Marry, B. Noetinger, C. Nieto-Draghi, and B. Rotenberg, Mineral- and ion-specific effects at clay-water interfaces: Structure, diffusion, and hydrodynamics, J. Phys. Chem. C **122**, 18484 (2018).
[42] T. Mouterde and L. Bocquet, Interfacial transport with mobile surface charges and consequences for ionic transport in carbon nanotubes, Eur. Phys. J. E **41**, 148 (2018).
[43] X. Geng, M. Yu, W. Zhang, Q. Liu, X. Yu, and Y. Lu, Slip length and structure of liquid water flowing past atomistic smooth charged walls, Sci. Rep. **9**, 18957 (2019).
[44] C. Pean, B. Daffos, C. Merlet, B. Rotenberg, P.-L. Taberna, P. Simon, and M. Salanne, Single electrode capacitances of porous carbons in neat ionic liquid electrolyte at 100 °C: A combined experimental and modeling approach, J. Electrochem. Soc. **162**, A5091 (2015).
[45] Y. M. Liu, C. Merlet, and B. Smit, Carbons with regular pore geometry yield fundamental insights into supercapacitor charge storage, ACS Cent. Sci. **5**, 1813 (2019).
[46] N. Ganfoud, A. Sene, M. Haefele, A. Marin-Laflèche, B. Daffos, P.-L. Taberna, M. Salanne, P. Simon, and B. Rotenberg, Effect of the carbon microporous structure on the capacitance of aqueous supercapacitors, Energy Storage Mater. **21**, 190 (2019).
[47] T. Méndez-Morales, N. Ganfoud, Z. Li, M. Haefele, B. Rotenberg, and M. Salanne, Performance of microporous carbon electrodes for supercapacitors: Comparing graphene with disordered materials, Energy Storage Mater. **17**, 88 (2019).
[48] J. D. Cyran, M. A. Donovan, D. Vollmer, F. Siro Brigiano, S. Pezzotti, D. R. Galimberti, M.-P. Gaigeot, M. Bonn, and E. H. G. Backus, Molecular hydrophobicity at a macroscopically hydrophilic surface, Proc. Natl. Acad. Sci. U.S.A. **116**, 1520 (2019).
[49] F. Creazzo, D. R. Galimberti, S. Pezzotti, and M.-P. Gaigeot, DFT-MD of the (110)-Co_3O_4 cobalt oxide semiconductor in contact with liquid water, preliminary chemical and physical insights into the electrochemical environment, J. Chem. Phys. **150**, 041721 (2019).
[50] S. Plimpton, Fast parallel algorithms for short-range molecular dynamics, J. Comput. Phys. **117**, 1 (1995).
[51] See Supplemental Material at http://link.aps.org/supplemental/10.1103/PhysRevLett.125.014501 for further details, which includes Refs. [52–58].
[52] A. I. Jewett, Z. Zhuang, and J.-E. Shea, Moltemplate a coarse-grained model assembly tool, Biophys. J. **104**, 169a (2013).
[53] W. Humphrey, A. Dalke, and K. Schulten, Vmd: Visual molecular dynamics, J. Mol. Graphics **14**, 33 (1996).
[54] A. Kohlmeyer, Topotools, https://zenodo.org/badge/latestdoi/13922095 (2017).

[55] L. Bocquet and J. L. Barrat, Hydrodynamic boundary conditions, correlation functions, and Kubo relations for confined fluids, Phys. Rev. E **49**, 3079 (1994).
[56] L. Bocquet and J.-L. Barrat, On the Green-Kubo relationship for the liquid-solid friction coefficient, J. Chem. Phys. **139**, 044704 (2013).
[57] T. A. Niehaus, S. T. Melissen, B. Aradi, and S. M. V. Allaei, Towards a simplified description of thermoelectric materials: accuracy of approximate density functional theory for phonon dispersions, J. Phys. Condens. Matter **31**, 395901 (2019).
[58] O. V. Yazyev and S. G. Louie, Electronic transport in polycrystalline graphene, Nat. Mater. **9**, 806 (2010).
[59] L. Joly, F. Detcheverry, and A.-L. Biance, Anomalous ζ Potential in Foam Films, Phys. Rev. Lett. **113**, 088301 (2014).
[60] M. Elstner, D. Porezag, G. Jungnickel, J. Elsner, M. Haugk, T. Frauenheim, S. Suhai, and G. Seifert, Self-consistent-charge density-functional tight-binding method for simulations of complex materials properties, Phys. Rev. B **58**, 7260 (1998).
[61] J. L. Abascal and C. Vega, A general purpose model for the condensed phases of water: TIP4P/2005, J. Chem. Phys. **123**, 234505 (2005).
[62] Z. R. Kann and J. L. Skinner, A scaled-ionic-charge simulation model that reproduces enhanced and suppressed water diffusion in aqueous salt solutions, J. Chem. Phys. **141**, 104507 (2014).
[63] D. Biriukov, O. Kroutil, and M. Předota, Modeling of solid-liquid interfaces using scaled charges: Rutile (110) surfaces, Phys. Chem. Chem. Phys. **20**, 23954 (2018).
[64] G. Pérez-Hernández and B. Schmidt, Anisotropy of the water-carbon interaction: Molecular simulations of water in low-diameter carbon nanotubes, Phys. Chem. Chem. Phys. **15**, 4995 (2013).
[65] C. Herrero, T. Omori, Y. Yamaguchi, and L. Joly, Shear force measurement of the hydrodynamic wall position in molecular dynamics, J. Chem. Phys. **151**, 041103 (2019).
[66] S. K. Kannam, B. D. Todd, J. S. Hansen, and P. J. Daivis, How fast does water flow in carbon nanotubes?, J. Chem. Phys. **138**, 094701 (2013).
[67] A. Striolo, A. Michaelides, and L. Joly, The carbon-water interface: Modeling challenges and opportunities for the water-energy nexus, Annu. Rev. Chem. Biomol. Eng. **7**, 533 (2016).
[68] P. Montero de Hijes, E. Sanz, L. Joly, C. Valeriani, and F. Caupin, Viscosity and self-diffusion of supercooled and stretched water from molecular dynamics simulations, J. Chem. Phys. **149**, 094503 (2018).
[69] R. Qiao and N. R. Aluru, Atypical dependence of electro-osmotic transport on surface charge in a single-wall carbon nanotube, Nano Lett. **3**, 1013 (2003).
[70] C. I. Bouzigues, P. Tabeling, and L. Bocquet, Nanofluidics in the Debye Layer at Hydrophilic and Hydrophobic Surfaces, Phys. Rev. Lett. **101**, 114503 (2008).
[71] M.-C. Audry, A. Piednoir, P. Joseph, and E. Charlaix, Amplification of electro-osmotic flows by wall slippage: Direct measurements on OTS-surfaces, Faraday Discuss. **146**, 113 (2010).
[72] B. Siboulet, S. Hocine, R. Hartkamp, and J.-F. Dufréche, Scrutinizing electro-osmosis and surface conductivity with molecular dynamics, J. Phys. Chem. C **121**, 6756 (2017).
[73] A. H. Castro Neto, F. Guinea, N. M. R. Peres, K. S. Novoselov, and A. K. Geim, The electronic properties of graphene, Rev. Mod. Phys. **81**, 109 (2009).
[74] D. Zhan, J. Yan, L. Lai, Z. Ni, L. Liu, and Z. Shen, Engineering the electronic structure of graphene, Adv. Mater. **24**, 4055 (2012).
[75] G. Tocci, L. Joly, and A. Michaelides, Friction of water on graphene and hexagonal boron nitride from ab initio methods: Very different slippage despite very similar interface structures, Nano Lett. **14**, 6872 (2014).
[76] B. Grosjean, M.-L. Bocquet, and R. Vuilleumier, Versatile electrification of two-dimensional nanomaterials in water, Nat. Commun. **10**, 1656 (2019).
[77] G. Tocci, M. Bilichenko, L. Joly, and M. Iannuzzi, *Ab initio* nanofluidics: Disentangling the role of the energy landscape and of density correlations on liquid/solid friction, Nanoscale **12**, 10994 (2020).
[78] F. Mouhat, F.-X. Coudert, and M.-L. Bocquet, Structure and chemistry of graphene oxide in liquid water from first principles, Nat. Commun. **11**, 1566 (2020).
[79] B. N. J. Persson, U. Tartaglino, E. Tosatti, and H. Ueba, Electronic friction and liquid-flow-induced voltage in nanotubes, Phys. Rev. B **69**, 235410 (2004).
[80] A. Vanossi, N. Manini, M. Urbakh, S. Zapperi, and E. Tosatti, Colloquium: Modeling friction: From nanoscale to mesoscale, Rev. Mod. Phys. **85**, 529 (2013).
[81] J. B. Sokoloff, Enhancement of the water flow velocity through carbon nanotubes resulting from the radius dependence of the friction due to electron excitations, Phys. Rev. E **97**, 033107 (2018).